VYSOKÉ UČENÍ TECHNICKÉ V BRNĚ
Fakulta chemická
Ústav chemie materiálů

RNDr. Vladimír Čech, Ph.D.

**PLASMA POLYMER FILMS PREPARED BY
PLASMA-ENHANCED CHEMICAL VAPOR DEPOSITION**

**TENKÉ VRSTVY PLAZMOVÝCH POLYMERŮ PŘIPRAVENÉ Z
PLYNNÉ FÁZE V PLAZMATU**

SHORT VERSION OF HABILITATION THESIS

VUTIUM

Brno 2001

Key Words

thin films, plasma polymerization, space-charge-limited currents, amorphous silicon, interface/interphase

Klíčová slova

tenké vrstvy, polymerace v plazmatu, proudy omezené prostorovým nábojem, amorfní křemík, mezifáze

Místo uložení práce

Areálová knihovna VUT v Brně
Purkyňova 118, Brno

Contents

Curriculum Vitae

Born: August 24, 1959 in Znojmo

Education: 1978-1983   Fac. of Science, Masaryk Univ. Brno (in field: physical electronics)
1983   RNDr. in field of physical electronics and optics (Masaryk Univ.Brno)
1998   Ph. D. in field of materials engineering (Brno Univ. of Technology)

Employment: 1983-1985   CHIRANA Stará Turá (Technical Assistant)
1985-1996   VTÚO Brno (Research Worker)
1996-   Fac. of Chemistry, Brno Univ. of Technology (Assistant Professor)
1997-2000   Secretary of the Institute of Materials Chemistry
2000-   Deputy Head of the Institute of Materials Chemistry

Scientific interests:
preparation, characterization and application of thin films
mechanical, electrical and optical properties of thin films
fiber-reinforced polymer composites (FRC)
surface treatment and modification of fibres for FRC
amorphous semiconductors
ionizing radiation, detection, semiconductor detectors

Membership in scientific societies:
Materials Research Society (USA)
International Plasma Chemistry Society (Switzerland)
Union of Czech Mathematicians and Physicists („R)

Publications: 46 papers in journals and conference proceedings
19 research reports

Teaching: Practice from structure and properties of polymer materials
Practice from technology of composite materials
Thin polymer films and polymer surfaces

1 Introduction

Some thin-film deposition processes use molecular gases and vapors, rather than solid evaporants or sputter targets, as their source materials. These processes are generally referred to as "chemical vapor" deposition processes, implying that the starting gases/vapors are "chemically activated" before deposition. In plasma-enhanced chemical vapor deposition (PECVD), chemical activation is achieved by supplying electrical power to a gas/vapor at reduced pressure, typically between 10^0 and 10^2 Pa. At these pressures, the application of a sufficiently high voltage creates a visible glow, called glow discharge plasma. The plasma consists of about equal concentrations of ions and free electrons (quasi-neutral particle system), frequently also containing neutral particles (atoms, molecules). The visible glow is caused by charge recombination processes and the relaxation of electronically excited atoms and molecules. Plasmas are frequently subdivided into low- and high-temperature plasmas. A further subdivision relates to thermal and non-thermal plasmas (Table 1, T_e and T_i are temperatures of free electrons and ions, respectively). Glow discharges belong to the non-thermal low-temperature plasmas.

Table 1. Subdivision of plasmas [1].

Low-temperature plasma		High-temperature plasma
Thermal $T_e \approx T_i \approx T \approx 2 \times 10^4$ K	Non-thermal $T_i \approx T \approx 300$ K $T_i \ll T_e \lesssim 10^5$ K	$T_i \approx T_e \gtrsim 10^7$ K
e.g., arc plasma at normal pressure	e.g., low-pressure glow discharge	e.g., fusion plasmas

The electrical power is coupled into the gas/vapor through the mediation of plasma electrons. The energetic electrons in the plasma ionize the gas, if only to a minor extent B about one part per million. A much larger fraction of the gas, about 1 percent, is chemically activated by the electrons. The increased chemical activity of the gas/vapor results primarily from dissociation of the molecules into smaller species, called radicals. Radicals are chemically unsaturated and therefore capable of chemical reactions at high rates; they are the species that react at a surface and contribute to film formation.

One can simply picture the PECVD process as a sequence of three distinct processes: the chemical activation of a gas/vapor molecule through electron impact dissociation, the transport of the radical species to the substrate, and the chemical reaction at the film surface.

The relatively light electrons present in the plasma are easily accelerated by the electric field. The same electrical force acts on the ions but they are much heavier and accelerate slower. Electrons do not lose much energy in most collisions with the background gas. Low-energy electrons collide elastically with the gas/vapor molecules due to the large mass difference between the electrons and gas/vapor molecules. A plasma electron can therefore accumulate more and more energy in the electric field. Once an electron has gained enough energy, an inelastic collision may take place. The free electron loses energy and the molecule increases its energy and often dissociates. In such an inelastic collision, the electron loses several electron volts of energy to the gas/vapor molecule. This energy can cause a gas/vapor

molecule to rotate and vibrate; it can also electronically excite the gas or cause it to dissociate or ionize. Many of these inelastic interactions increase the "chemical activity" of the gas/vapor molecules by several orders of magnitude. The ensemble of plasma electrons is characterized by a (nearly) Maxwellian electron energy distribution [2].

The mean electron temperature of a typical glow discharge is equivalent to an energy between 1 and 3 eV. This energy must be compared to the energy needed to dissociate or ionize the gas, an energy range roughly between 3 and 20 eV. Therefore, only the electrons in the high-energy tail of the distribution chemically activate and ionize the molecular gas. It takes much less electron energy to dissociate a molecule and form two neutral fragments that it takes to overcome the strong coulombic forces to produce an ion and electron pair. The shape of electron energy distribution suggests that there are far more plasma electrons with the relatively low energies at which radicals can be formed than there are electrons capable of ionizing the gas/vapor. Indeed, in a PECVD plasma, the density of neutral radicals is much higher than the density of ions but a physically correct argument should also take the various cross sections into account.

Gas flow velocities in most practical PECVD systems are so low that neutral radicals created in the plasma find their way to the surface of the film by diffusion. The concentration gradient driving the diffusion process is maintained by radical generation in the plasma and their disappearance at the film surface. This concentration gradient exists over a linear dimension approximately corresponding to width of the dark space or sheath. For reasonable estimates of the diffusion coefficients, one can calculate deposition rates to be typically of the order of 10Å s^{-1}, in agreement with observations [3]. Much higher deposition rates can be obtained in the directional flows of convective systems. These systems require special gas inlets, flow patterns, and high pump speeds.

2 Hydrogenated Amorphous Silicon

The "sand" resources of silicon are almost unlimited, a factor that makes a technology based on this material very interesting. In contrast to the well-developed high technology of crystalline silicon (c-Si), the amorphous silicon (a-Si) thin film technology opens a new field of low cost and large area application possibilities.

Chittick and co-workers (1969) [4] developed the preparation of a-Si by plasma-enhanced decomposition of silane gas. This method results in hydrogenated a-Si (a-Si:H), a material with the sufficiently low density of states (DOS) in the mobility gap. Therefore the electrical properties of a-Si:H can be varied over a wide range by n- and p-type substitution doping in a systematic and reproducible manner [5]. The doping possibility has led to a huge increase in activity in this field not only in basic research but also in application development.
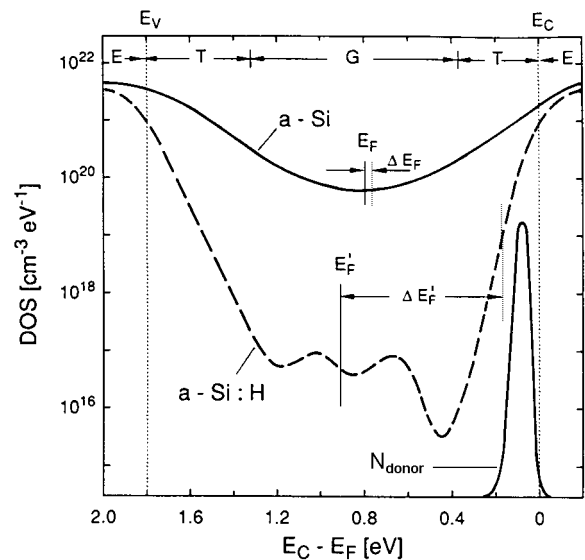

Figure 1. Fundamental distribution of the DOS for a-Si and a-Si:H. As an example the shift in the Fermi level E_F due to incorporation of donors (density N_{donor}) is shown: E, extended states; T, tail states; G, gap states; E_V and E_C are mobility edges of the valence or the conduction band respectively.

The first *p-n* junction and the first solar cell on the a-Si:H material have already been reported in 1976. Today the conversion stable efficiency of a-Si:H-based solar cells has exceeded 11% (the goal is 16% stable efficiency) and numerous non-photovoltaic applications have been developed.

The description of the electronic properties of a-Si:H starts with the energy distribution of electronic states. Depending on their energy and character, the different states determine the electrical transport, recombination and doping, etc. Some effects of disorder in a-Si:H on the electronic states are broadening of the density of states distribution compared to the crystal to form the band tails; the localization of the band tail states; and the reduction of the scattering length to atomic distances. It is convenient to divide an energy-dependent density of states distribution, *N(E)* into three different energy ranges; the main conduction and valence bands, the band tail region close to the band edge, and the defect states in the forbidden gap (Fig. 1 [6]).

2.1 Steady-state space-charge-limited currents -numerical simulation

One-carrier steady-state space-charge-limited currents (SCLC) enable the determination of the bulk energy distributions of localized states for undoped and/or slightly doped a-Si:H. SCLC measurements are mostly made on sandwich structures of the metal-semiconductor-metal type with both contacts being ohmic for electrons or holes or, in the case of n^+-i-n^+ (p^+-i-p^+) devices, with heavily doped contact layers to improve the injection of electrons (holes) into the intrinsic layer. Voltage applied to such a structure establishes a one-carrier current. In case of an n^+-i-n^+ structure, the electrons are injected from the n^+ layer (injecting contact) into the intrinsic region and the counter n^+ layer blocks the injection of holes (and vice versa for a p^+-i-p^+ structure). Injected nonequilibrium electrons populate empty trap levels above the thermal equilibrium Fermi level E_{F0} during the release time τ_R. This follows from the principle of detailed balance when quasi-thermal equilibrium between free and trapped electrons is achieved and the new quasi-Fermi level E_F is shifted towards the conduction band edge. The extra free and trapped electrons form excess space-charge that controls the steady-state current given by the mobile electrons. The space-charge is determined by the distribution of the trap levels and the Fermi function. An energy diagram for an n^+-i-n^+ structure calculated by the author [7] is depicted in Fig. 2.

The basis of the SCLC method was set by the work of Rose [8] and Lampert and Mark [9,10]. These authors have shown that the plot of current-voltage (*I-V*) characteristics reflects the trap levels and, in principle, the trap level parameters can be extract from nonlinearities of that plot.

Pfister [11] derived parametric equations for construction of *I-V* curves on the basis of the space-charge and the free carrier densities and derived relations for back extraction of these quantities from the *I-V* characteristics. Following previous work, Manfredotti *et al*. [12] determined equations for an evaluation of SCLC measurements without an a priory assumption about the nature of the energy distribution. Stöckmann [13] refined this method and the same was done by Weisfield [14]. This way
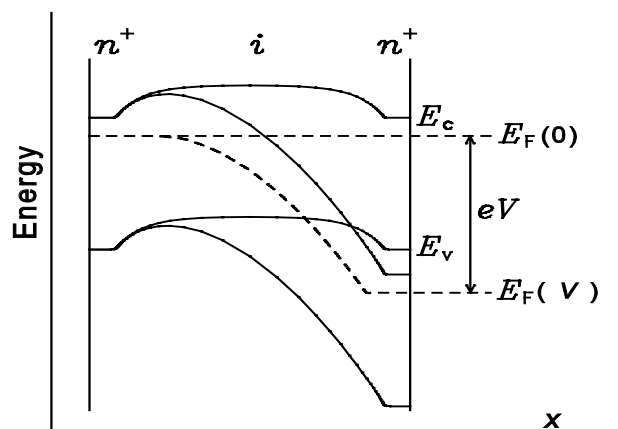

Figure 2. Schematic diagram for an n^+-i-n^+ structure at zero bias and at a bias of *V*.

of analysis uses higher order (up to the third order) derivatives of the *I-V* characteristics and in order to avoid fluctuations, some simple versions were proposed [12,13]. Nešpçrek and Sworakowski [15-17] proposed a similar differential method including the first derivatives of *I-V* curve only. The simple and practical formula for determination of arbitrary trap distributions from the SCLC measurements were given by den Böer [18].

The SCLC measurements are typically made on sandwich n^+-i-n^+ structures, where the heavily doped contacts layers (n^+) allow carriers to move freely into the undoped (*i*) layer. In order to verify the standard SCLC assumptions of the space-charge-limited currents
(1) the microscopic mobility μ_0 is field independent,
(2) diffusion currents are neglected and therefore we can write for the current density

$$J = e \ \mu_0 n(x \ ) F \ (x \ ), \tag{1}$$

where n is the density of free electrons and F is the electric field strength,
(3) there is an infinite reservoir of free electrons at the injecting contact (n_c (x=0)64, F(x=0) = 0; "the virtual cathode approximation"),
(4) there is a spatially homogeneous trap distribution throughout the intrinsic layer,
a numerical simulation would be available.
Realistic modelling of an n^+-i-n^+ a-Si:H structure requires the simultaneous solution of the complete set of transport equations. Owing to ohmic contacts the current through the structure is formed by single carriers - electrons. Therefore the transport equations are the Poisson equation

$$\frac{d \ F}{d \ x} = \frac{\rho(x \ )}{\varepsilon \ \varepsilon_0}, \tag{2}$$

where the space-charge density, ρ, as a function of the quasi-Fermi energy can be expressed as

$$\rho(E_F) = - e \int_E N (E \ ) [f (E - E_F) - FUNCf (E - E_{F0})] dE, \tag{3}$$

f $(E - E_F)$ is the Fermi function, the electron continuity equation

$$\frac{dn}{dt} = \frac{1}{e} \frac{dJ}{dx} + G (x) - R (x) \tag{4}$$

(*G* is the generation rate, *R* is the recombination rate) and electron current-density equation

$$J = J_{dr} + J_{dif} = e \ \mu_0 n (x) F (x) + e D \frac{dn (x)}{dx}, \tag{5}$$

where *D* is the diffusion coefficient *D* = μ_0 *kT/e* (Einstein relation). The author solves the steady-state single-carrier transport and therefore d*n*/d*t* = 0, *R* = 0, and without any generation, i.e., *G* = 0. It follows

8

from (4) that $\mathrm{d}J/\mathrm{d}x = 0$ and thus $J = $ const along the structure.

It seems that a solution of transport equations without any simplification is not easy. Several approaches have been published. Tredgold used diffusion currents to calculate J-V characteristics already in 1966 [19]. Grinberg and Luryi [20] presented an analytical solution. They replaced Eqs. (2), (3) and (5) by approximative relations and found I-V characteristics in a parametric form. Other authors have not avoided approximative relations either. For instance, numerical simulations of Pfleiderer *et al.* [21] for a suitable function $N(E)$, or of Tehrani *et al.* [22] for a discrete trap level. Hack and Shur [23,24], Hack and den Böer [25] and Wentinck *et al.* [26,27] solved complete set of transport equations for electrons and holes including recombination. Their modelling was developed for a *p-i-n* structure, as well as for *n-i-n* and *p-i-p* structures. Hack and Shur have used the zero-temperature statistics and Wentinck *et al.* have solved transport equations for a set of discrete trap levels. Their models seem to be quite realistic, however, Wentinck and co-workers obtained plots of model J-V characteristics quite different of those derived under the standard SCLC assumptions, which is surprising. Spatial profiles at the junctions (*n-i*, *i-n*, *p-i*, *i-p*) were not correct either.

Therefore, the author have looked for a more realistic model [7]. A solution of the Poisson equation with respect to the potential, φ, was substituted by a solution with respect to a perturbation of the potential, $\delta\varphi$.

Let $a = x_1 < x_2 < ... < x_N = b$ is a mesh on the x-axis. The mesh points are not equally spaced. Instead, the grid spacing decreases gradually closer to junction between differently doped layers because of the large potential and electron density gradients at these junctions. For each iteration step k, a new estimation for the potential $\varphi^{k+1} = \varphi^k + \delta\varphi^k$ is calculated from the application of Newton's iteration principle to the Poisson equation . For this calculation, the Taylor expansion theorem is applied to the nonlinear functions in the Poisson equation disregarding the higher-order terms. Substitution of $\varphi^{k+1} = \varphi^k + \delta\varphi^k$ in the Poisson equation (2) yields the matrix equation

$$\mathrm{A} \ \delta\varphi^k = \mathrm{b}, \tag{6}$$

where A is a tridiagonal matrix with elements

$$a_{j,j-1} = \frac{2}{(\Delta x_{j-1} + \Delta x_j)\,\Delta x_{j-1}}$$

$$a_{j,j} = -\frac{2}{\Delta x_j\,\Delta x_{j-1}} - \frac{e^2}{\varepsilon\,\varepsilon_0\,kT}\left[n + kT \int_{E_v}^{E_c} N(E)\frac{\mathrm{d}\,f(E-E_F)}{\mathrm{d}(E-E_F)}\mathrm{d}E\right] \tag{7}$$

$$a_{j,j+1} = \frac{2}{(\Delta x_{j-1} + \Delta x_j)\,\Delta x_j}$$

with $\Delta x_j = x_{j+1} - x_j$, $j = (1, ..., N\text{-}1)$ and the element b_j of a vector b is

9

$$b_j = -\frac{2\left(\dfrac{\varphi_{j+1}-\varphi_j}{\Delta x_j} - \dfrac{\varphi_j-\varphi_{j-1}}{\Delta x_{j-1}}\right)}{\Delta x_{j-1} + \Delta x_j} +$$

(8)

$$+ \frac{e}{\epsilon\epsilon_0}\left\{ n - n_0 + \int_{E_v}^{E_c} N(E)[f(E-E_F) - f(E-E_{F0})]\,\mathrm{d}E \right\}$$

The matrix A is a nearly symmetric positive definite matrix with diagonal dominance. Therefore, the usual iterative solution methods are convergent, see e.g., Ralston [19].

If a spatial profile of the potential, $\varphi(x)$, is known for the above mesh, one can calculate the current density through the structure as

$$J = \frac{\mu_0 kT\left\{ n(b) - n(a)\exp\left[\dfrac{e(\varphi(b)-\varphi(a))}{kT}\right]\right\}}{\exp\left[\dfrac{e(\varphi(b)-\varphi(a))}{kT}\right]\displaystyle\int_a^b \exp\left[\dfrac{-e(\varphi(x)-\varphi(a))}{kT}\right]\mathrm{d}x}.$$

(9)

To find a spatial profile of the density of free electrons, $n(x)$, arecurent formula have to be used

$$n(x_{j+1}) \cong \exp\left[\frac{e(\varphi(x_{j+1}) - \varphi(x_j))}{kT}\right] n(x_j) +$$

$$+ \frac{J}{2\mu_0 kT}\left\{ 1 + \exp\left[\frac{e(\varphi(x_{j+1}) - \varphi(x_j))}{kT}\right]\right\}\Delta x_j$$

(10)

By means of a Newton iteration scheme the current-density equation and the Poisson equation are evaluated subsequently (under boundary conditions) until convergence is obtained. For each iteration step, k, first the current density, J^k, going through the structure is calculated using Eq. (9) and the density of free electrons, $n^k(x)$, along layers is evaluated by means of Eq. (10) for a given $\varphi^k(x)$. This calculation is followed by the calculation of a new estimation for the potential $\varphi^{k+1} = \varphi^k + \delta\varphi^k$ from the Poisson equation. The boundary conditions are as follows: $\varphi(a) = V$, $\varphi(b) = 0$, $n(a) = (n_0)_n$, $n(b) = (n_0)_n$, where $(n_0)_n$ is the free electron density at thermal equilibrium for the n layer.

For a spatially homogeneous DOS $(h(E,x) = N(E).S(x)$, where $S(x) = 1)$ and parameters given in Table 2, the potential profiles, the electric-field profiles, the space-charge density profiles and the $E_F - E_c$ profiles are illustrated in Fig. 3 [7]. These profiles are calculated for an n^+-i-n^+ structure at zero bias (curve a) and at a bias of $V = 1.1$ V (curve b), 4.8 V (curve c), 11.1 V (curve d).

10

Table 2. Parameters used in the program NIN for the description of the n^+-i-n^+ structure.

|		
Temperature	T	250 K
Conductivity prefactor	σ_{min}	120 Ω^{-1} cm^{-1}
Relative dielectric constant	ε	12
Free electron mobility	μ_0	12 cm^2 V^{-1} s^{-1}
Conduction band	E_c $N(E_c)$	0.00 eV 2.9H10^{21} cm^{-3} eV^{-1}
Conduction band tail	T_c	300 K
Valence band	$E_c - E_v$ $N(E_v)$	1.8 eV 2.9H10^{21} cm^{-3} eV^{-1}
Valence band tail	T_v	600 K

Dangling bonds
    D^0
    i layer
    D$^-$
 	
    n layer   D$^-$
	$(E_c - E_{db}{}^0)_i$
	$(N_{db}{}^0)_i$
	$(\sigma_{db}{}^0)_i$
	$(E_c - E_{db}{}^-)_i$
	$(N_{db}{}^-)_i$
	$(\sigma_{db}{}^-)_i$
	$(E_c - E_{F0})_i$
	$(E_c - E_{db}{}^-)_n$
	$(N_{db}{}^-)_n$
	$(\sigma_{db}{}^-)_n$
	$(E_c - E_{F0})_n$
		0.85 eV
		5.0H10^{15} cm^{-3} eV^{-1}
		0.10 eV
		0.55 eV
		5.0H10^{15} cm^{-3} eV^{-1}
		0.10 eV
		0.70 eV
		0.55 eV
		3.0H10^{18} cm^{-3} eV^{-1}
		0.10 eV
		0.25 eV

Donor state	$E_c - E_{donor}$ N_{donor} σ_{donor}	0.10 eV 3.5H10^{18} cm^{-3} eV^{-1} 0.07 eV
Thickness of i layer	L	2.0 μm
Thickness of n layer	L_n	0.1 μm
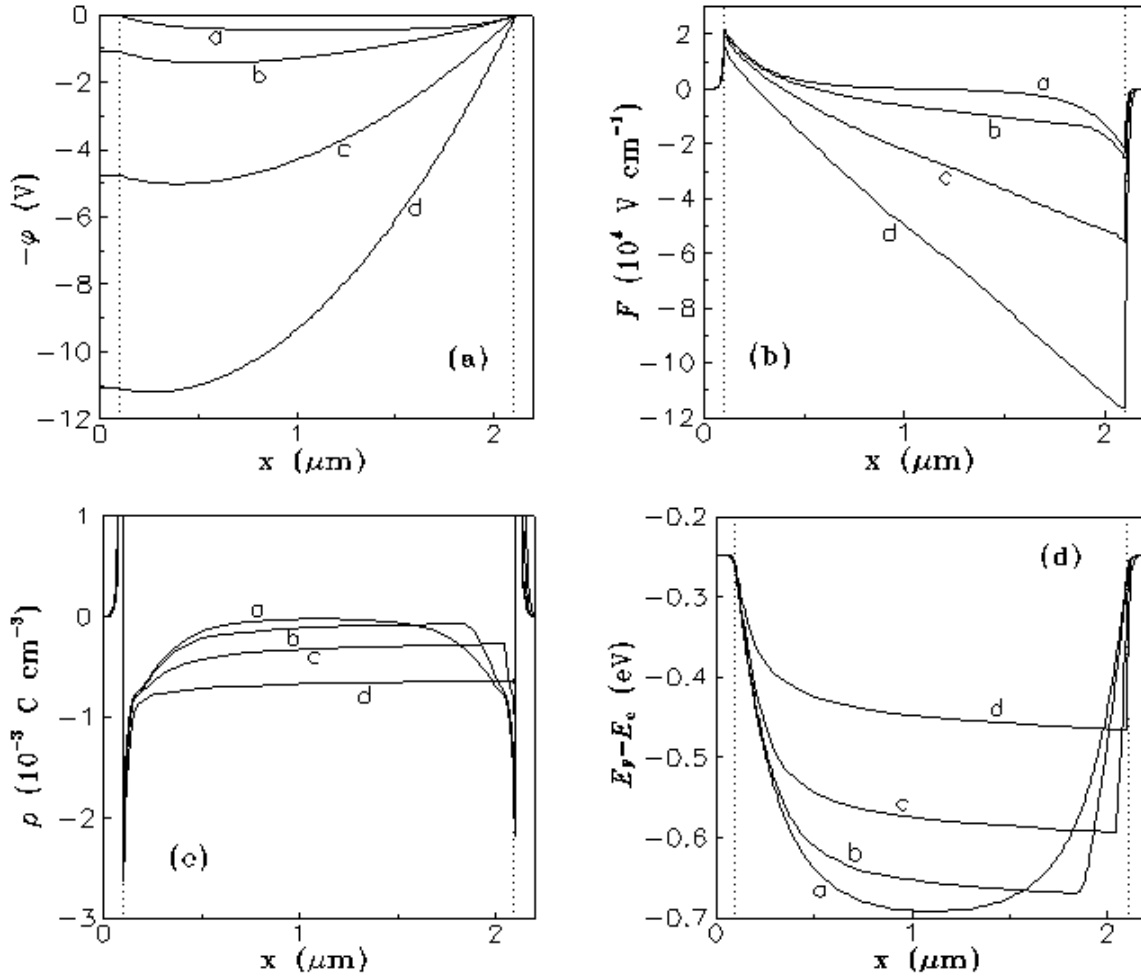
Figure 3. (a) The potential, (b) the electric field, (c) the space charge and (d) the energy profiles in an n^+-i-n^+ structure at zero bias (curve a) and at different applied voltages: 1.1V - curve b, 4.8V - curve c, 11.1V - curve d.

Fig. 4a shows the modelled current density - voltage (J-V) characteristics for the homogeneous density of defect states $(N_{db}^0)_i = (N_{db}^-)_i = (N_{db})_i = 5.0 \times 10^{15}$ cm^{-3} eV^{-1} (device quality a-Si:H), respectively, and for the i layer thickness $L = 1.0$ μm (curve a), 2.0 μm (curve b) and 5.0 μm (curve c). These J-V characteristics were calculated including diffusion currents, see dashed lines (index: 1), and without diffusion currents, see solid lines (index: 2). The lower density of defect states in the band gap of undoped a-Si:H the larger extent of space charge (band bending) into a bulk of the i layer. (E_F - E_c) profiles (Fig. 4b) are calculated for an n^+-i-n^+ structure at thermal equilibrium. Differences between corresponding J-V characteristics (between
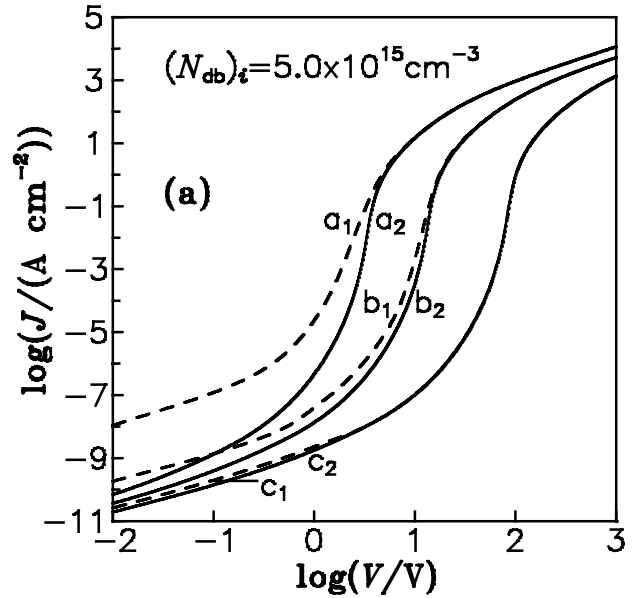
the dashed and the solid line) are due to diffusion currents. The *J-V* characteristics have approximately the same plot if the drift currents dominate over most of the bulk of an *i* layer.

It can be expected that the junction between the n^+ layer and the *i* layer is not abrupt for a real n^+-*i*-n^+ structure. Therefore, the author included a spatial DOS distribution in his model calculations with quite new and important results [7].

2.2 Time relaxation of space-charge-limited conductivity

The author studied [20,21] the relaxation of the space-charge-limited (SCL) conductivity due to the space-charge decay and showed that the time dependence of the conductivity is DOS-dependent at long times. The study continued the previous one of Solomon [22].

sufficiently low bias, V_0 (# 0.1 V), applied across such an n^+-i-n^+ device, practically does not change the equilibrium conductivity, σ_0, of the undoped a-Si:H (Fig. 5). However, using a higher bias V_L (e.g. 1 V) results in an injection of electrons that are trapped on localized states above the equilibrium Fermi energy, E_{F0}, and which form the space charge along the undoped layer. The space-charge-limited conductivity decreases till the steady-state value, $\sigma_{ss}(V_L)$, is reached. The new quasi-equilibrium between the free and the trapped electrons is characterized by the quasi-Fermi energy, E_F, which is shifted towards the conduction band. The same applies to any arbitrary bias V_H (> V_L), e.g. 10 V. Now if the bias V_H drops (at time $t = 0$) to the previous value, V_L, the potential barrier due to the space charge decreases the conductivity of the device to the value σ_1 (Fig. 5). The trapped electrons are thermally excited back into the conduction band, decreasing gradually the barrier and the SCL conductivity relaxes to its steady-state value, $\sigma_{ss}(V_L)$, as experimentally demonstrated in Figs. 6, 7.

According to the study, the time relaxation of SCL conductivity at long times $(t/\tau_R(E_F) > 3)$ is given by
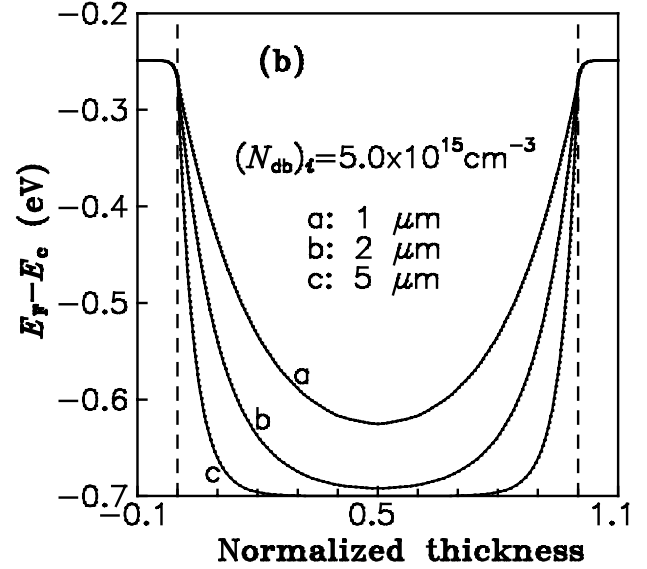

Figure 4. (a) Modelled *J-V* characteristics with (dashed lines) and without (solid lines) diffusion currents at a defect density of $(N_{db})_i = 5.0 \times 10^{15}$ cm^{-3} and at an *i* layer thickness of $L = 1.0$ μm (curve a), 2.0 μm (curve b) and 5.0 μm (curve c). (b) Energy profiles at zero bias and at different thicknesses of
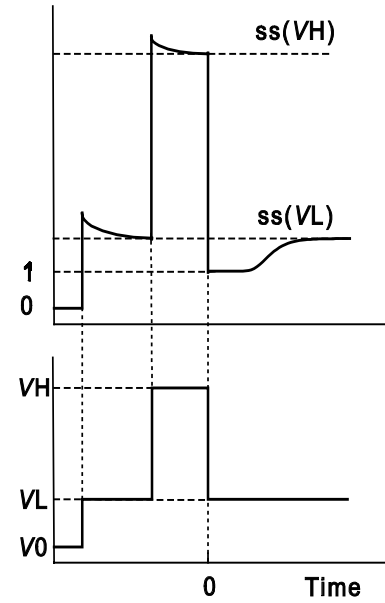

Figure 5. Schematic diagram of the conductivity varying with bias and time for an n^+-i-n^+ device.

13

$$\sigma\,(t)\,\_\,\sigma_{ss}\,\exp\left[-\frac{1}{8}\frac{e^2 L^2 N(E_F)}{\varepsilon\,\varepsilon_0}\frac{1}{\nu_0}\exp\left(\frac{E_C - E_F}{kT}\right)\frac{1}{t}\right], \tag{11}$$

and the release time, τ_R, is

$$\tau_R(E) = \nu_0^{-1}\exp\left(\frac{E_{FUNCC} - E}{kT}\right), \tag{12}$$

where ν_0 is the attempt-to-escape frequency, and E_C is the conduction band edge.

According to Eq. 25 the increase in SCL conductivity depends on the density of states at the quasi-Fermi energy, $N(E_F)$, and on E_F energy position. This relation could therefore be used to determine the density of states and, increasing the bias V_L and hence enhancing the energy E_F, the energy distribution of DOS could be evaluated. This idea was a basis of the new method derived and tested by the author in Ref. 21.
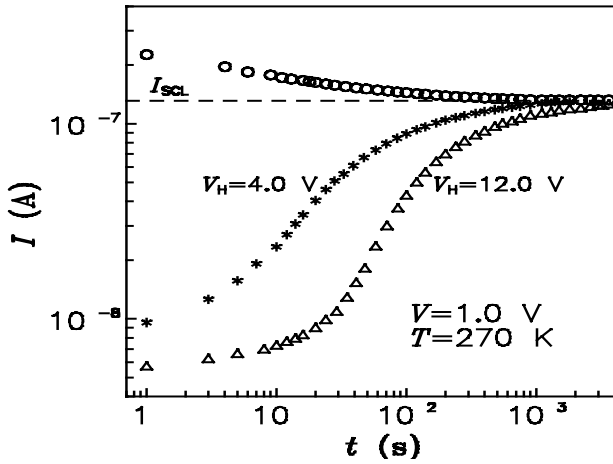

Figure 6. An illustration of the current relaxation to the steady-state value, I_{SCL}.
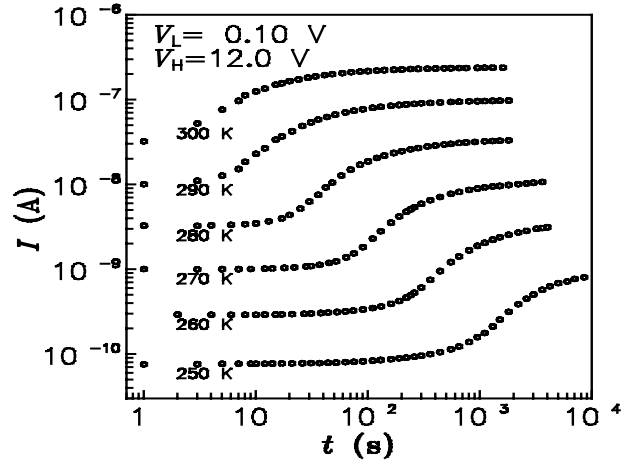
Figure 7. Time relaxation of the current after injection at different temperatures.

3 Plasma-Polymerized Organosilicones

We consider in this chapter only films produced from `organicA source compounds, even if the resulting thin film deposits turn out to have `inorganicA characteristics. This can result from co-reaction in the plasma of an organosilicon compound with oxygen or ammonia, for example, or from PECVD of the pure vapors at elevated substrate temperatures, or their combination. The starting monomers contain at least three different atoms (Si, C, and H for plasma-polymerized tetramethylsilane (pp-TMS), or vinyltrimethylsilane (pp-VTMS), for example), and in many cases four (for example O or N, in addition to the three mentioned above, for plasma-polymerized hexamethyldisiloxane (pp-HMDSO) or hexamethyldisilazane (pp-HMDSN)). In extreme cases, the starting molecule may even contain five different atoms (e.g., Si, C, H, N, and O in γ-Aminopropyltriethoxysilane) [23-25].

The very special interest which has existed since the earliest days of plasma chemistry for the organosilicones may be attributed to a number of reasons [26]:

1) This chemical family, comprising many hundreds of compounds, includes several dozen which are sufficiently volatile near ambient temperature to be used with relative ease in normal plasma-chemical procedures,

2) Organosilicones tend to be relatively nontoxic, and they are generally of low flammability or nonflammable, relatively cheap, and available from commercial sources.

3) Conventional organosilicon polymers and elastomers play an important role in macro-molecular science, both from the fundamental and applied points of view. It is therefore logical that researchers should be interested in exploring plasma-generated counterparts to these materials.

4) Last, but not least, modern semiconductor technology is largely based on the use of silicon. The natural chemical affinity between pure, single-crystalline silicon and organosilicon plasma polymers has motivated much device-oriented research.

Table 3. Main organosilicon precursors and conditions used to growth plasma films [27].

Name	Plasma source	Pressure range (Pa)	Power range (W)
Hexamethyldisiloxane	RF, μW, LF	$10^{-1} ! 10^2$	3 ! 100
Tetraethoxysilane	RF, μW	$10^{-1} ! 10^2$	3 ! 100
Tetreamethyldisiloxane	13.56 MHz Inductive coupling	1.3	25
Divinyltetramethyldisiloxane	13.56 MHz Capacitive coupling remote plasma	$10^0 ! 10^1$	14 ! 200
Methyltrimethoxysilane	13.56 MHz Capacitive coupling	14.6	300
Octamethylcyclotetrasiloxane	13.56 MHz Capacitive coupling remote plasma	$10^0 ! 10^1$	14 ! 200
Bis(Trimethylsilyl)methane	13.56 MHz Inductive coupling	1.3	50 ! 150
Hexamethyldisilane	13.56 MHz Inductive coupling	1.3	50 ! 150
Tetramethylsilane	13.56 MHz Inductive coupling	1.3	25
Hexamethyldisilazane	13.56 MHz Extern. Electr.	33.3	7
Tris(dimethylamino)silane	ECR (2.45 Ghz)		1000
Hexamethylcyclotrisilazane	20 kHz Capacitive coupling	26.6	$2\,mA/cm^2$

The monomers are sometimes used alone but more often in mixtures with a rare gas like argon and also an active gas (O_2, N_2O for example). In the latter case it is generally admitted that the atomic oxygen is created in the plasma phase and that this atomic oxygen reacts in the gas and at the plasma-surface interface with the organic parts of the organosilicon precursor. In such a case the aim is to realize the inorganic films of the type SiO_x or Si_xN_y.

Table 3 shows some organosilicon precursors used in plasma technology. From 1 to 6, the precursors present at least one SiBO bond in their structure. The last one (number 6) is cyclic. Precursors

1 and 4 are very similar. HMDSO is the most utilized, however TMDSO presents the advantage of having a weak SiBH bond, easily dissociable in the plasma and an expected higher deposition rate (SiBH bond: 71 kcal/mol, SiBC bond: 104 kcal/mol). From 7 to 9 the monomer composition does not contain any oxygen or nitrogen atom, thus addition of oxygenated or nitrogenated gas is necessary to obtain SiBO or SiBN bond in the deposited layer. From 11 to 12 all the precursors present at least one SiBN bond in their chemical structure. The last one (number 12) is cyclic. All the precursors listed in the table have been used under plasma conditions.

The films realized from organosilicones have remarkable optical, mechanical and electrical properties resulting in the development of their applications in the fields of protective coatings, scratch resistant films, planar light guides, dielectric films for capacitors or intermetallic insulation in integrated circuits.

3.1 Plasma-polymerized dichloro(methyl)phenylsilane

Plasma polymer layers of the thickness ranging from 10^{-2} to 10^{0} μm intended to engineer interphases in glass-fiber reinforced polymer composites and single-layer light-emitting diodes were prepared by RF glow discharge technique, see the author>s results in Ref. 28. The films synthesized from a mixture of dichloro(methyl)phenylsilane (DCMPS) vapor and gaseous hydrogen were deposited on flat glass and silicon substrates and glass fibers as well. Deposition conditions were optimized to obtain required thickness, mechanical and electrical properties of interphases. Prepared layers were amorphous, relatively rigid and transparent at room temperature with excellent adhesion to substrates. The surface of plasma polymer is rough with isolated (silicon substrate) and conglomerate (glass substrate) grains. FTIR and XPS spectra revealed a great amount of atomic oxygen bound to silicon atoms and enabled to determine the atomic concentrations. The structure model is proposed assuming a random carbosiloxane network with not-crosslinked methyl and phenyl groups.

Plasma polymer films of the thickness from 80 nm to 7 μm were prepared. The mean deposition rate of 0.3 nm s^{-1} was determined from the thickness measurement and the corresponding deposition time.

The typical absorption IR spectrum of pp-DCMPS is compared with those of the spin coated PMPS and the monomer (DCMPS) in Fig. 8.

Atomic concentrations in pp-DCMPS and PMPS films determined from XPS spectra are
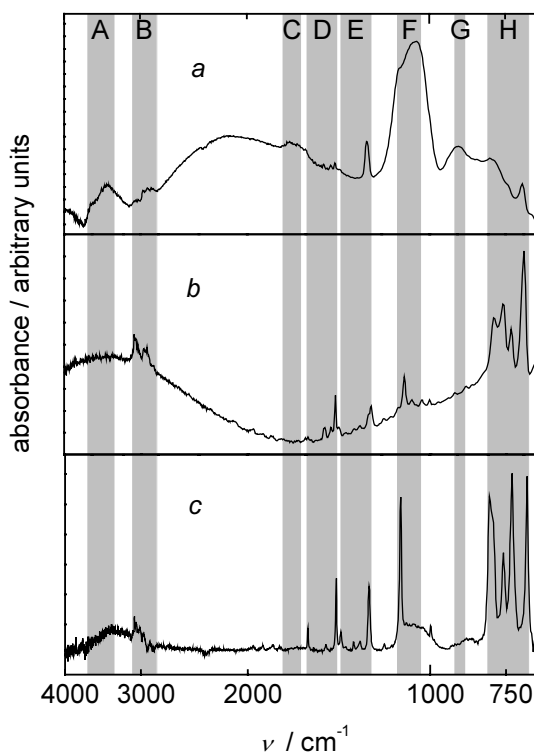

Fig. 8. FTIR spectra: (a) plasma polymer (pp-DCMPS), (b) spincoated PMPS, (c) monomer (DCMPS).

16

shown in Table 4. A use of Mg K_α radiation gives results more surface-sensitive. However, the measurements do not indicate a depth inhomogeneity. The mean element ratios are $n(C)/n(Si) = 4.8$ and $n(O)/n(Si) = 1.9$ in pp-DCMPS films and $n(C)/n(Si) = 4.7$ and $n(O)/n(Si) = 0.8$ in spin coated PMPS films in contrast to the monomer $n(C)/n(Si) = 7$. Binding energies of Si 2p, C 1s, and O 1s corresponding to the plasma polymer were 101.8B102.0 eV, 283.9B284.0 eV, and 531.8B531.9 eV, respectively. The binding energy of Si 2p was assigned to OBSiBO bonds and that of C 1s may be assigned to SiBCH$_3$ and/or SiB(C$_6$H$_5$) and/or SiBCH$_2$BSi bonds. It is assumed the great amount of oxygen in the plasma polymer originates from the oxygen-contaminated monomer (see IR spectrum) and subsequent postdeposition oxidation [29].

Table 4. Atomic Concentrations Determined from XPS Spectra

Polymer	Radiation	Atomic mole fraction / %			
		C	O	Si	Cl
pp-DCMPS	Mg K_α	60.4	25.7	12.9	0.9
pp-DCMPS	Al K_α	63.1	23.4	12.8	0.6
PMPS	Mg K_α	72.8	11.8	15.4	-

Surface morphology of pp-DCMPS films on various substrates is depicted in Fig. 19. Scanning electron micrograph in Fig. 9*a* shows a rough surface of the film on a polished Si substrate. Grains of different size up to 1 μm are randomly dispersed across the surface and some grains can stick together. A height of the grains reaches up to 30 nm as it follows from measurements of surface profiles by the Talystep technique. Areas of such a high roughness are alternated by areas with a low roughness (4 nm). Similar grain structure was observed at SEM micrographs obtained from the edge of a film on broken substrate that is an indication of a material toughness. The grain structure observed at plasma polymer surfaces [30B32] is apparently connected with the plasma polymerization mechanism. There are conglomerations of grains of different sizes on the whole surface of a film deposited on microscope cover glass (Fig. 9*b*). Scratches on the glass surface as nucleation centers are probably the cause of grains coordinated in straight lines. Similar conglomerations of grains can be seen on the surface of a glass fiber coated with pp-DCMPS (Fig. 9*c*). The spin coating technique enables to prepare homogeneous PMPS films of a thickness ranging from 100 nm to 1 μm with a smooth surface. A low roughness of 1 nm was determined using the X-ray reflectivity.
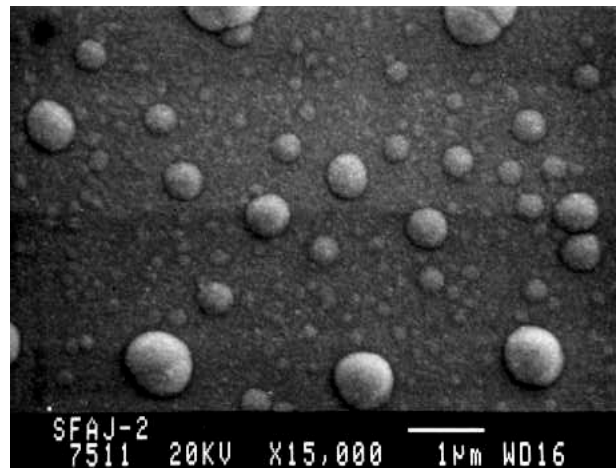
pp-DCMPS films exhibit excellent adhesion not only to glass substrates and silicon wafers, but even to metal substrates and organic materials (PE, PP, PC, Teflon). The simple adhesion test using the plasma polymer film with a cross-shaped scratch immersed in boiling water was carried out for the silicon substrate and no peeling of the coated layer was observed after 8 h indicating a remarkable adhesion. The deposition conditions were optimized to enhance the adhesion characterized by the scratch tester up to a normal loading of 18 N. It is assumed the adhesion of plasma polymer films to substrates results from siloxane bonds. An adhesion of the spin-coated PMPS to the same substrate is poor with a normal loading < 1 N outside the measuring range of the tester.

Composites consisting of the plasma polymer layer (t_{film} = 4.1 μm) and the PP foil (t_{PP} = 100 μm) were used to determine the Young's modulus of plasma polymer at room temperature, E_{film} = (6.0 " 0.5) GPa. This value is higher than those of bulk conventional polymers (up to 3 GPa) and of the plasma polymer prepared from tetramethylsilane (TMS) (3 GPa [24]).

In an additional study [33], some of samples were annealed in vacuum up to temperatures ranging from 450 to 700 °C. Chemical composition, structure and surface morphology of annealed samples and those

Fig. 9. Scanning electron micrographs of plasma polymer films on (a) silicon wafer, (b) microscope cover glass,

stored in air at room temperature were studied by FTIR, XPS, SEM, and optical microscopy. Thermal stability and decomposition of the plasma polymer with increasing temperature were characterized using thermogravimetry together with mass spectrometry. The plasma polymer was stable up to a temperature of 300 °C. Above that temperature the material started to decompose together with additional cross-linking due to the incorporation of extra oxygen atoms forming new siloxane bonds. The plasma polymer was tough at room temperature but much more brittle after annealing.

As it was mentioned above, the IR spectra (Fig. 8) revealed a great number of siloxane bonds in the film, which may be connected with a post-deposition oxidation as plasma polymers are known to be susceptible to oxidation after fabrication. There may be a great number of free radicals in the freshly prepared material and the free radicals initiate oxidation by reacting with in-diffusing atmospheric O_2. Therefore, we may expect an increase of oxygen atoms at the surface of a plasma polymer film. However, the depth profile of oxygen concentrations in Fig. 10 showed a great number of oxygen atoms across the whole film. It means that the deposition chamber was contaminated with a rest of water molecules embedded on the chamber wall, which resulted in the incorporation of oxygen atoms into the plasma polymer during deposition.

An abrupt change in the concentrations of carbon and silicon atoms at the surface (Fig. 10) can be
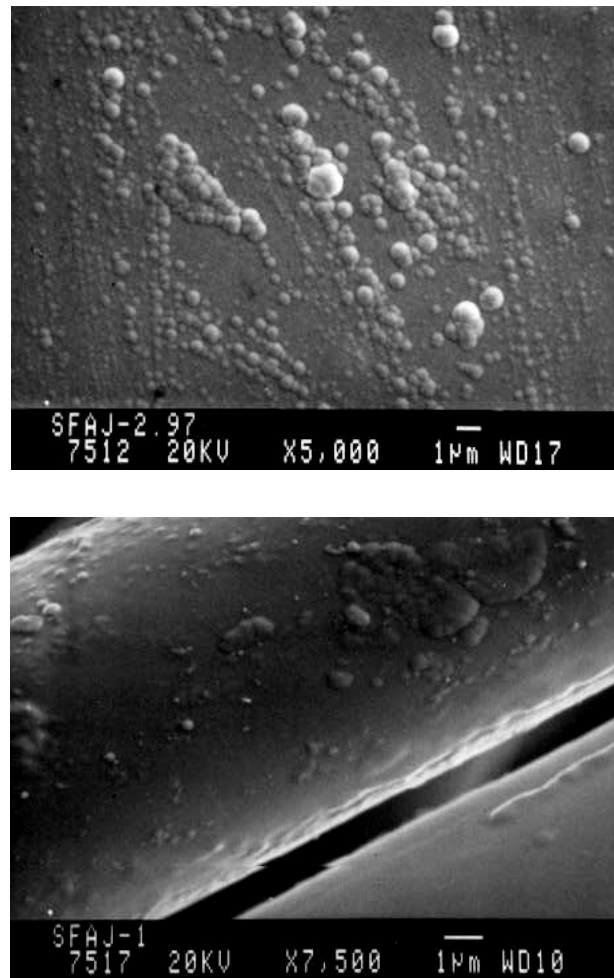
18

explained as follows: There is no reason to expect great changes in the number of silicon atoms across the film. This assumption means that the numbers of carbon and oxygen atoms at the surface are higher than those in the bulk of the film, as it corresponds to element ratios (Fig. 10). The surface element ratios are $n(C)/n(Si) = 5.8$ and $n(O)/n(Si) = 2.3$ while after the first sputtering they are $n(C)/n(Si) = 3.4$ and $n(O)/n(Si) = 1.5$. Therefore, there may be a layer of a thickness of 3B4 nm at the surface with different chemical composition and structure. The value $n(C)/n(Si) = 5.8$ is close to a monomer ratio of 7.0 and it can be underestimated as the XPS observed layers are 6B8 nm thick.

Fig. 10. Depth profiles of atomic concentrations across the plasma polymer film together with element ratios. Interfaces of the film are marked out. Thickness of the deposited film was 1.4 μm.

With respect to the deposition process we know that monomer vapor is still in the chamber for a short time after the glow discharge is switched off. Hence, monomer molecules are not fragmented and can react with a deposited polymer, which contains many free radicals, and/or can be physisorbed on the surface, which may explain the high number of carbon atoms at the surface. The surface layer of films stored in the open air can react with atmospheric humidity - postdeposition oxidation (rest of chlorine atoms react with water molecules), which may explain the high number of oxygen atoms at the surface.

Results of thermal analysis (Fig. 11) showed that weakly bonded methyl and phenyl groups released the plasma polymer if elevated temperatures are used and this fact is confirmed by the IR spectra. A reduction of carbon atoms at the surface of annealed films is also evident from the XPS analysis (Fig. 12). The atomic concentration of silicon atoms for the sample annealed up to 700 °C seems to be overestimated as the XPS analysis was influenced by the Si substrate and in fact, the ratio of $n(O)/n(Si)$ increases with temperature. Thus, the reduction of carbon atoms seems to be compensated by oxygen atoms. As reported by Assink *et al.*, [34] the heat treatment of plasma-polymerized hexamethyldisiloxane (pp-HMDSO) films in air forms additional siliconBoxygen bonds. According to their NMR study [34] the number of oxygen atoms increased with temperature and most
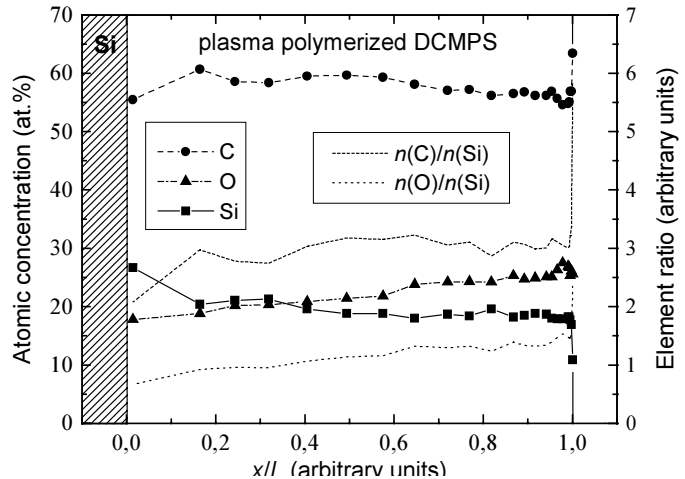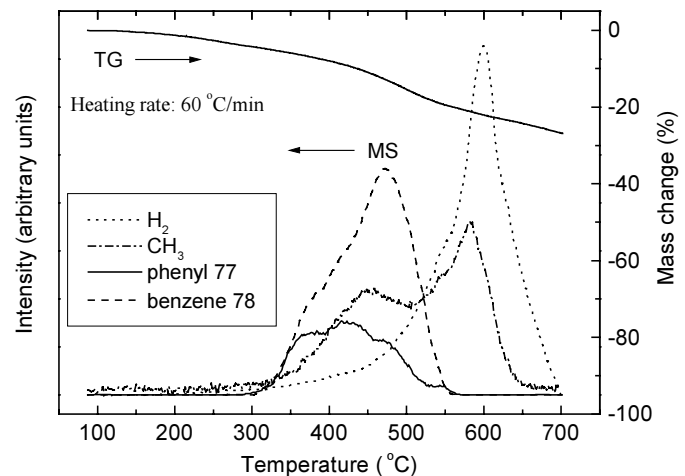

Fig.11. Thermogravimetric (TG) characteristics compared with mass spectrometry (MS) ones to identify released species during thermal decomposition of the plasma polymer.

19

of the monofunctional silicones were replaced by tri- and tetrafunctional ones. By analogy with the pp-HMDSO, additional cross-linking of the plasma polymer material can be expected for the annealed pp-DCMPS. Silicon atoms with free bonds can react with the oxygen ones, increasing the crosslinking of the polymer as weakly bonded methyl and phenyl groups are released from the heated material. The Si!C bonds are, therefore, replaced by the Si!O ones at elevated temperatures. Such a highly crosslinked material should be brittle and this mechanical property was observed at broken films using optical microscopy [33].

Fig. 12. Atomic concentrations and element ratios as a function of annealing temperature.

The last question is as follows: How can the extra oxygen be incorporated in the bulk of the annealed film if heat treatment was carried out in vacuum? Experimental and model studies realized by Klaptchenko [35] with water sorption of the pp-DCMPS films suggested that the plasma polymer has a highly-dispersive and microporous structure. The interaction of the material with water was very strong and the structure exhibited swelling and time relaxation as reported in Ref. 55. The volume fraction of pores was about 6% in normal laboratory conditions and the value increased with relative humidity [35]. Sorbed water in our specimen was confirmed by the IR spectrum for a sample stored at room temperature. Water molecules in a porous bulk of pp-DCMPS film can, therefore, be the source of extra oxygen atoms incorporated into a highly-crosslinked network of the annealed material. Atomic force microscopy (AFM) was employed to identify the pores but with no definite results.

3.2 Plasma-polymerized hexamethyldisiloxane

We have developed the inductively coupled system for deposition of thin plasma polymer films on solid substrates in RF discharge (40 MHz). The thin films were prepared from vapor of hexamethyldisiloxane (HMDSO) at low RF power to reduce the aging effect in deposited films [36]. The monomer has a relatively simple chemical structure to study the influence of deposition conditions on film properties. The plasma-polymerized (pp) films exhibited an excellent adhesion to the glass substrate. The strong and hydrolytically stable bond could be employed in fiber-reinforced polymer composites if the pp-HMDSO film would be used for surface modification of glass fibers. The pp-HMDSO films were characterized by many techniques suitable to investigate their mechanical and thermal properties, and to determine chemical composition, structure and surface morphology.
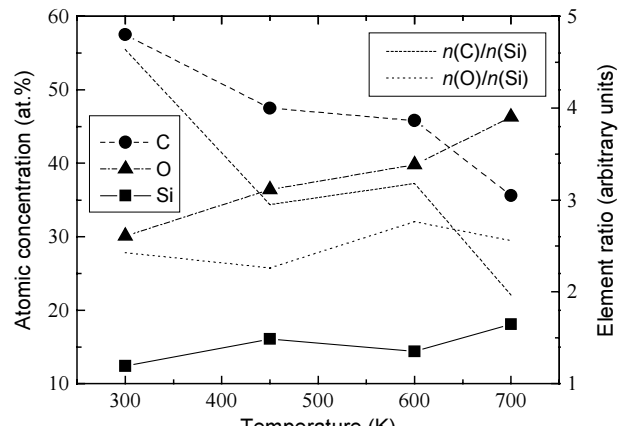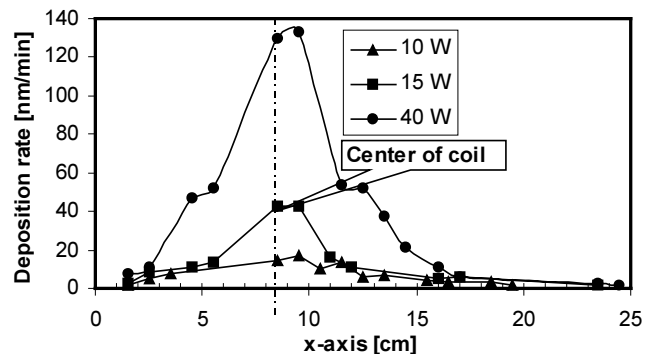

Fig. 13. Distribution of deposition rate along the reactor chamber

20

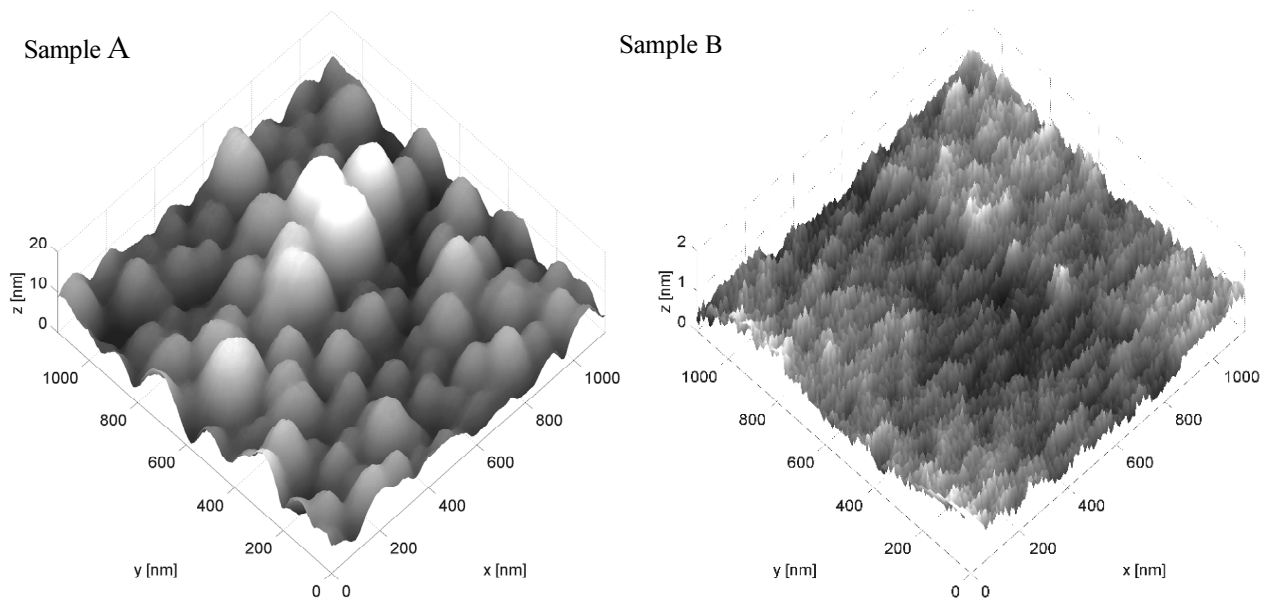Sample A   Sample B

Fig. 14. AFM images of two samples: sample A was placed under the generator coil, sample B was positioned 150 mm from the coil center.

The thin films were deposited on silicon wafers, glass slides and PET foils at different deposition conditions, such as RF power (< 40 W), time of deposition and flow rate. We have studied distributions of the deposition rate along the chamber axis as a function of RF power (Fig. 13).

Atomic force microscopy (AFM) together with scanning electron microscopy (SEM) were used to observe the surface morphology and to evaluate the roughness of prepared films. The surface profiles of two different films are plotted in Fig. 14. We measured the sample (A), which was situated at the center of plasma discharge. The thickness of the film was 4.0 μm and the roughness was 20 nm. The second sample (B) with the thickness of 320 nm and roughness of 2 nm was placed 130 mm from the center of
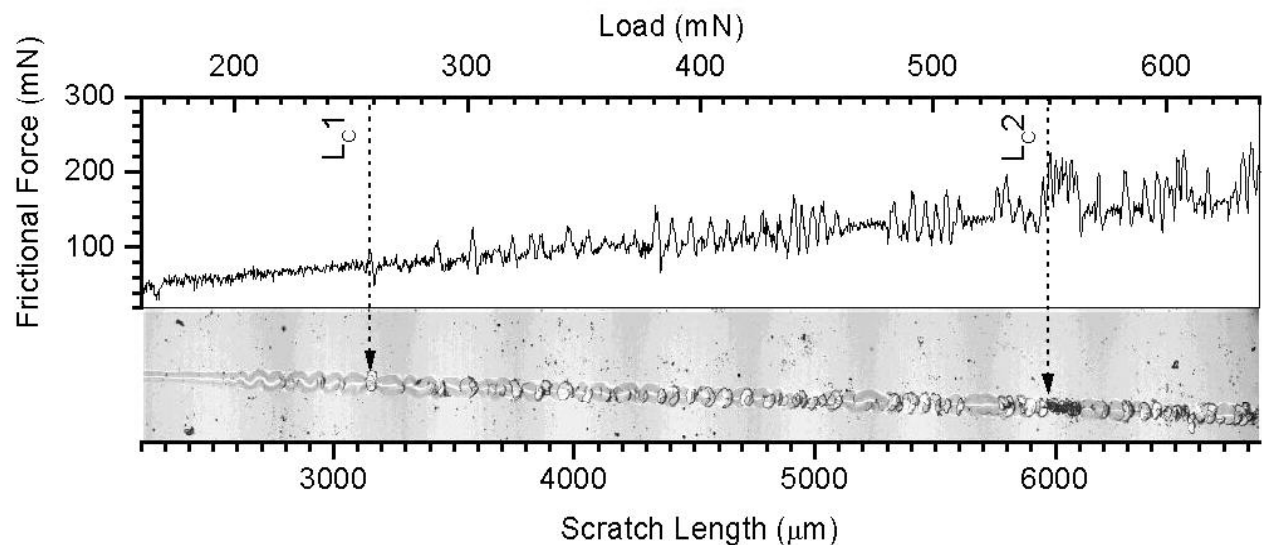

Fig. 15. Scratch in plasma polymer film together with scratch test record.

21

plasma discharge.

A qualitative indication of the adhesion of the thin pp-HMDSO films deposited on Si wafers at different deposition conditions has been tested using boiling distilled water for 8 hours. After this time the samples were taken out and the adhesion was observed to be excellent. A widely used method of evaluating the adhesion of films is a scratch test. Therefore, we have developed a scratch-tester in our institute. A scratch in pp-film formed by the diamond tip together with typical scratch recording of load profile is depicted in Fig. 15.

The surface free energy [37,38], its disperse and polar parts, of pp-HMDSO layers deposited on glass slides was estimated on a basis of contact angles measurements against distilled water, ethylenglykol, glycerol and methyleniodide, Table 5.

Table 5. Contact angle and surface free energy estimated according to Wu and OWRK (Owends-Wendt-Rabel-Kaelbe) methods.

Power [W]	Contact angle [°]		Surface free energy [mJ/m^2]					
	Glycerol	Methyleniodide	Total		Polar		Dispersive	
			Wu	WRK	Wu	WRK	Wu	WRK
7	95,4	65,7	27,8	25,0	24,9	24,4	3,0	0,4
10	90,3	61,1	30,4	28,3	25,8	26,9	4,9	1,4
30	91,7	62,1	29,8	27,6	25,8	26,7	4,0	1,0
40	92,1	62,2	29,6	27,6	25,9	26,8	3,7	0,8

The modulus of layers was estimated using the tensile test of the two-layer composite system that consists of plasma polymer film (pp-HMDSO) and thin substrate (8 μm thick PET foil). E_{PET} changes with temperature and that is why the foil was exposed under the deposition conditions. The pp-film modulus was found to be $(1,0 \pm 0,2)$ GPa (Fig. 16).
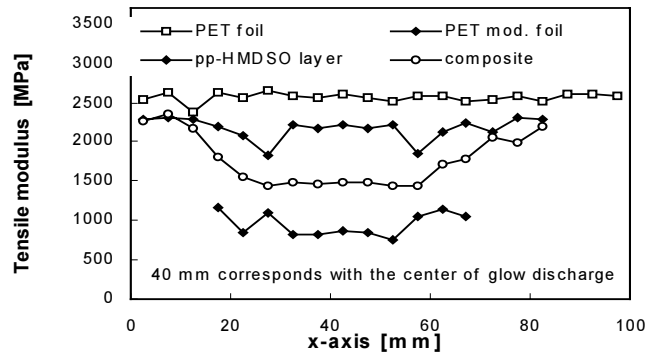

Fig. 16. PP-HMDSO modulus as a function of the position in the plasma chamber.

3.3 Plasma surface treatment and modification of fibers for polymer composites

A development of high-performance composites is tightly bound with a designing of composite interphases. The interphase is a region intermediate to the fiber and the matrix which are in a contact. In fact this region includes the fiber coating and a part of the matrix affected by the presence of the coated fiber. Theoretical and experimental studies have shown that the properties of fiber reinforced composites are given by the coating material with its thickness and modulus, by the interaction at interfaces with the fiber and the matrix, and by the reinforcement and matrix materials. Therefore, sophisticated interphases can lead to higher strength and higher toughness of the specific composite system. Low temperature plasma technology is the new technique used for surface modification of reinforcements. This technology is able to prepare controlled interphases [39].

Fiber reinforced composites combine high strength of rigid reinforcements with high toughness of flexible matrix. Synergism of the two phases produce mechanical properties of the composite material that cannot be achieved with either of the constituents acting alone, due to the presence of an interphase between the reinforcement and the matrix. The interphase is a region intermediate to the fiber and the matrix, the composition and/or structure and/or properties of which may be variable across the region and which also may differ from the composition and/or structure and/or properties of either of the two constituents [40,41]. This concept of the interphase is schematically illustrated in Fig. 17. We can distinguish two interfaces at the interphase region. One of them at the fiber surface (fiber/interphase) is relatively sharp and the other at the matrix (interphase/matrix) is a diffused one. If the surface of the fiber is modified by a coating (interlayer) there is the third inner interface between the interlayer and the modified matrix. Interphases influence and may control the mechanical properties of composites using fibers with a diameter of 10-25 μm and the common fiber volume fraction ranging from 0.5 to 0.7 as it is evident from experimental and model data. Therefore, the interphase properties are becoming gradually accepted as design and process variables to be tailored for particular end application
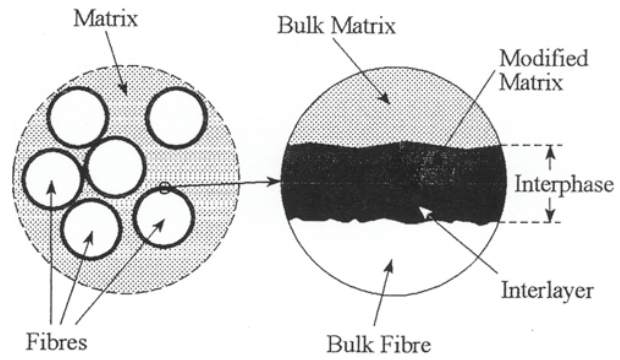

Fig. 17. Schematic ilustration of the composite

The primary function of the interphase is to transmit stress from the matrix to the fibers and to protect the fibers from environmental damage. An ability of this region to transmit stress depends upon the interphase strength, as well as the mechanical properties of fiber, matrix, interphase, and the bonding forces (adhesion) at interfaces. The nature of bonding is not only dependent on the atomic arrangement, molecular conformation and chemical constitution of all the phases, but also on the morphological properties of the fiber and the diffusivity of elements in each constituent. Adhesion in general can be attributed to mechanisms including, but not restricted to, adsorption and wetting, mechanical interlocking, electrostatic attraction, molecular entanglement, and hydrogen and chemical bonding. The surface of reinforcements has to be modified to improve wetting and adhesion to the matrix for sophisticated composites. A lot of techniques for surface treatment of fibers are known and they differ depending on the fiber nature (glass, carbon, aramid, polyethylene, etc.) [41]. In recent years, plasma techniques found great applications in a development of high-tech composites.

Using Ar, H_2, O_2, CO_2, NH_3 and air plasmas contacted with the surface of reinforcements, the

activated species initiate chemical and physical reactions at the surface causing alteration of surface properties and surface morphology. This process is called plasma surface treatment. When plasma interact with organic molecules in vapor, plasma polymers are formed, and all surfaces of substrates in the plasma zone are coated with the material. The process is called plasma surface modification and it is a coating technique.

Plasma surface treatment and modification of fibers and their application in fiber reinforced composites are widely used from the 1980s. A lot of theoretical and experimental studies are devoted to plasma treatment and plasma coating (polymerization) processes [43]. An insight into interphase functionality together with bonding forced at interfaces is very difficult. Therefore, scientists try to understand relations among chemical composition, structure, surface morphology, and mechanical properties of interphases, and how can be influenced by deposition parameters of plasma technology. First, effects of plasma treatments and coated plasma polymers are analyzed using optical, electron, and atomic force microscopies, infrared, photoelectron, ion spectroscopies, contact angle measurements, and many others methods. Then, the data are envisaged with those characterizing mechanical properties of interphases in model composites (fiber fracture test, pull-out test, microdroplet test, microindentation test [44]) B interfacial shear strength (IFSS), and/or in complete laminate (short beam shear test [41]- ASTM D2344) B interlaminar shear strength (ILSS). An influence of plasma surface modification on interphase and polymer composite properties is outlined for carbon, aramid, polyethylene, and glass fibers.

The tensile strength of single fibers can be decreased using intensive plasma treatment (high power and/or long treatment time) owing to the etching effect, as it was observed by Bettge and Hinrichsen [45] that treated polyethylene fibers with oxygen plasma. Since carbon fibers are easily damaged by the ablation effect, plasma polymers were coated on the fiber surface to avoid the loss of strength of the fibers. Weisweiler [46] have used a mixture of acetylene/air plasma to deposit a plasma polymer on commercial carbon fibers. The tensile strength increases till a film thickness of about 50 nm is reached (Fig. 18). It was proposed that the plasma coatings effectively heal some of the surface flaws of the fibers, and so the tensile strength increases. However, with increasing volume of the layer, the number of surface flaws is growing due to Griffith>s theory, resulting in a decrease of the tensile strength above about 50 nm layer thickness.   Plasma surface treatment of carbon fibers has been studied using air, O_2, CO_2, and NH_3 plasmas, and plasma polymers have been deposited using dioxane and xylene; acrylonitrile and styrene; aniline, pyridine, and benzene monomer [43]. Organic vapors, such as polyamide; polyimide;
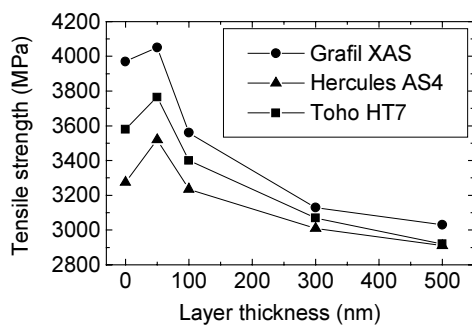

Fig. 18. Tensile strength of carbon fibres as a function of thickness of the plasma-polymer layer prepared from a mixture af acetylene vapor and air.
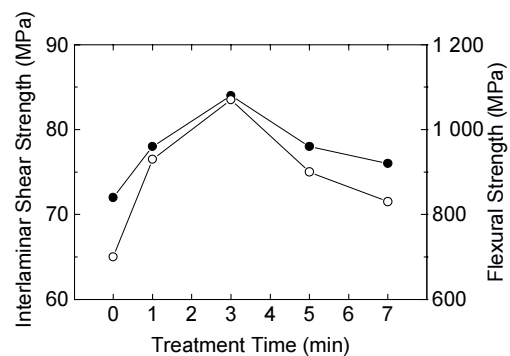

Fig. 19. Interlaminar shear strength () and flexuar strength () of carbon fibre/PEEK composites versus oxygen plasma treatment time.

organosilanes; styrene and maleic anhydride; propylene; and acrylonitrile and styrene were used as well [41]. Jang and Kim [47] have applied oxygen plasma treatment to modify an interphase in carbon fiber/PEEK composites. The interlaminar shear strength and the flexural strength as a function of plasma treatment time are shown in Fig. 19. It was confirmed that the mechanical properties of CF/PEEK composites are strongly influenced by the roughness of the carbon fiber surface and improved fiber wettability. A higher increase of ILSS can be found for carbon fiber/epoxy composites using organosilanes (Fig. 20) [41]. The improvement in interface bond strength was confirmed using microcomposite tests. However, all these beneficial effects of improved strength properties are inevitably accompanied by a loss in the impact fracture

Fig. 20. Effect of carbon fibre surface modification level on ILSS () and impact energy () for carbon fibre/epoxy composites.

toughness of unidirectional laminates (Fig. 20). Due to good bonding, debonding is more difficult and therefore the advancing crack propagates through the fibers, resulting in low impact strength. Hence a strong interface favors a brittle fracture with low energy absorption, whereas a weak interface favors multiple delaminations with high energy absorption. Furthermore, good adhesion exacerbates the physical mismatches which exist between the fibers and the matrix, increasing the stress concentration caused by imposed loads and/or thermal cycles. The fiber coating method for toughening composites seems to be one of the most effective methods for achieving simultaneously high strength and high toughness when an appropriate polymer is chosen [48]. Theoretical and experimental studies have shown that the coated material should be ductile or flexible with an interlayer modulus lower than that of the matrix [49] (Fig. 21) and that the layer thickness is very critical [50] (Fig. 22). The introduction of the flexible interlayer reduces or eliminates interfacial stresses, both under mechanical loading and temperature cycles and relieves the stress concentration into the matrix, resulting in improved mechanical performance, crack resistance and impact strength of the structural composite. Even thought it is not yet completely known which coating materials are most suitable for a specific composite system, the variables which affectthe properties of a fiber reinforced composites have been identified as follows: interlayer modulus, interlayer thickness, matrix modulus, coating material (composition), interaction at the interfaces [51].
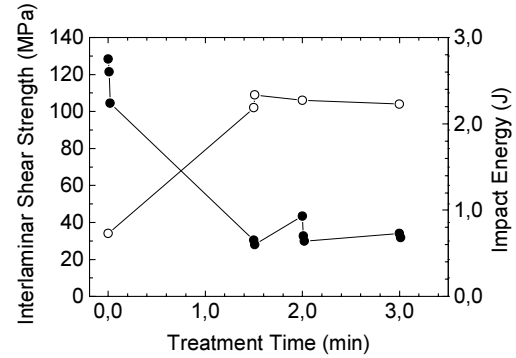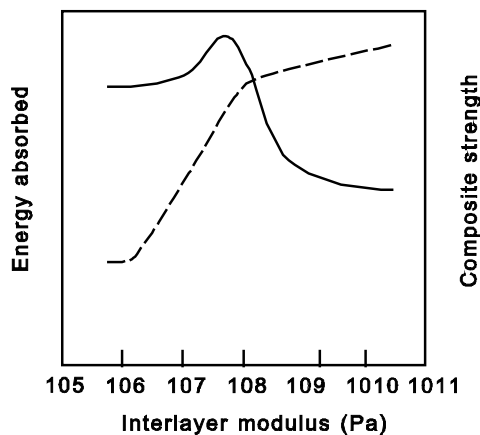
Fig. 21. Strain energy absorbed and composited strength as a function of interlayer modulus.
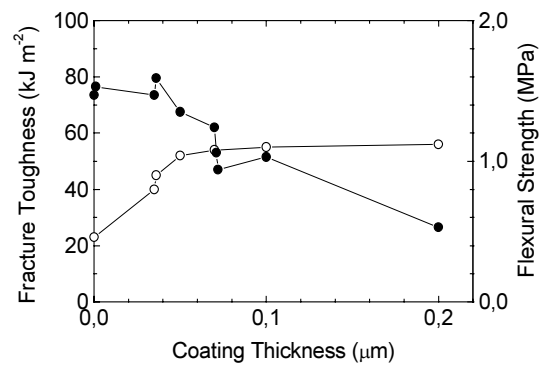
Fig. 22. Fracture toughness () and flexural strength () of silicone rubber coated carbon fibre/epoxy composites as a function of coating thickness.

The world market is dominated by *glass reinforcement* in *unsaturated polyester*, which comprises almost 90% of the total market. Approximately 1.8 H 10^6 t of E-glass fiber is manufactured annually for use in composites and 50% goes into continuous and long-fiber reinforced thermosets [52]. Commercially produced sizing is heterogeneous with respect to the thickness and uniformity [53], the molecules of silane coupling agents have a tendency towards self-condensation, forming siloxane oligomers rather than complete bonding with the glass surface [54,55], and the low density of siloxane bonds with the surface decreases if water

Fig. 23. Schematic diagram of plasma technology for continuous surface treatment and modification of fiber bundle.

molecules diffuse to the interface since this type of bond is hydrolytically unstable [56]. Only 10B20% of the total sizing is bonded to the fiber surface and this amount is directly related to the composite interfacial strength [57]. Technology centers in glass companies search for new ways of solving the above problems. One of the alternative technologies is the low-temperature plasma technique. This technique may be used as a gentle but powerful tool for the surface treatment and modification of fibers, which retain their mechanical properties.

New helical coupling plasma system for continuous surface treatment and modification of fiber bundles has been developed by author>s team and tested for glass fibers (Fig. 23 [58]). The system enables surface processing of single filaments and flat substrates as well. Surface processed glass fibers and their bundles were examined as reinforcements for glass fiber/polyester composite systems. Processing of fibers comprised a surface treatment using argon gas and a surface modification using hexamethyldisiloxane and vinyltriethoxysilane monomers. Plasma polymer films prepared from monomer vapors were widely characterized depending on process parameters. A low power density of < 0.4 W cm^{-3} is recommended for surface processing. Interfacial and interlaminar shear strengths of plasma processed glass fiber/polyester systems were compared with those of untreated and commercially sized fibers.

To determine the effects of surface treatment and modification on interphase functionality in glass fiber/polyester composite, microbond tests were performed and the interfacial shear strengths (IFSS) were calculated. Results for untreated and commercially sized (A-174) fibers are given in Fig. 24, together with results for surface modified (pp-HMDSO, pp-VTEO (vinyltriethoxysilane)) and treated (Ar-plasma) filaments. There are no functional groups at the surface of pp-HMDSO film and so the strength is similar to that for untreated fibers. Better results were obtained with pp-VTEO modification, as there is a low density of vinyl groups at film surface improving bonding with polyester resin. An improvement in IFSS is 33% for pp-VTEO modification with respect to untreated glass fibers. Interesting results were obtained for fibers treated in Ar-plasma and an IFSS increase is 38%. We can expect that improved wettability and increased roughness are the course of better adhesion at the fiber/matrix interface [47,59-60].

The interlaminar shear strengths (ILSS) of prepared short beams were evaluated using the four-point shear test. The ILSS values are depicted in Fig. 25. It is interesting that commercially sized fibers treated in Ar-plasma are of quite a good strength. The ILSS is higher by 66% in a comparison with untreated fibers. Low temperature plasma is recommended for cleaning processes [2]. However, we have revealed that commercially sized (A-174) glass fiber bundles are coated by plasma polymer of the same
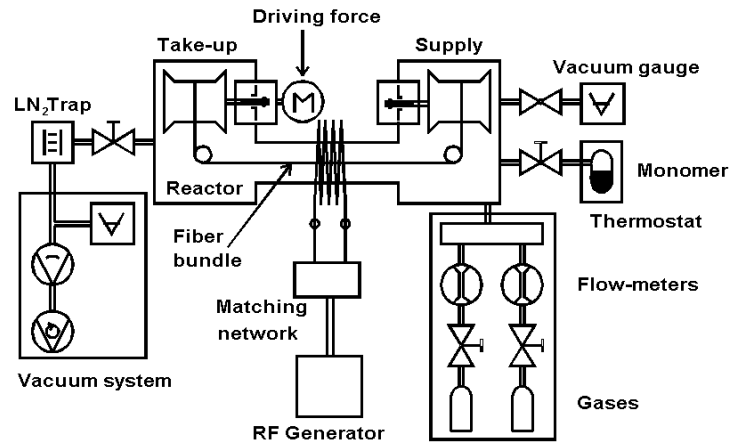
composition but different chemical structure after processing in Ar-plasma. The probable process comprises removing of the sizing, fragmentation and activation its molecules and deposition of highly crosslinked and irremovable plasma polymer.
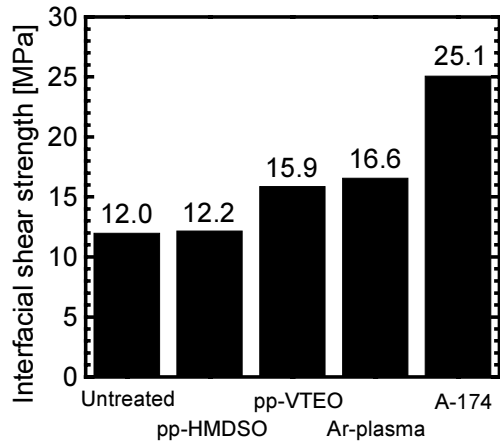

Fig. 24. Interfacial shear strength for surface-treated and modified fibers in glass fiber/polyester system.
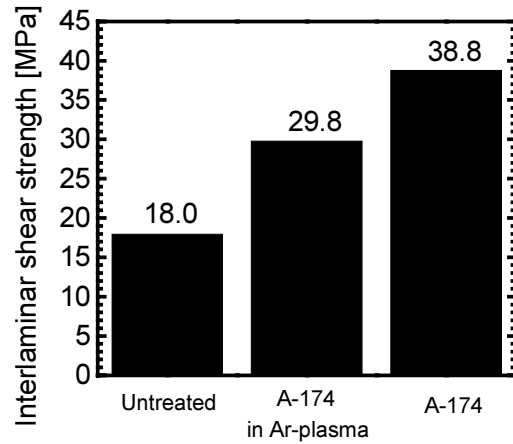

Fig. 25. Interlaminar shear strength of glass fiber/polyester composites with various surface processing of fibers.

4 Conclusion

Author's results are discussed in context with plasma-enhanced chemical vapor deposition. The thesis only indicate huge amount of interesting topics connected with research fields such as new materials, thin films, characterization techniques, plasma technology, vacuum science, etc. Most of the topics are interdisciplinary activities, which may be interesting for both the scientists and the engineers.

The hydrogenated amorphous silicon (a-Si:H) is a thin film semiconductor material with outstanding properties. It can be fabricated very easily and with low cost by different, mainly PECVD and PVD, methods. Effective doping of high quality material and the possibility of changing the energy gap by alloying, both of which can easily be done during the preparation process, enable a wide range of application potentialities. The author developed the successful tools for evaluation of steady-state and relaxation space-charge limited currents resulting in the density of states (DOS), the most important material parameter, and the attempt-to-escape frequency. The author>s model of n^+-i-n^+ structure enables calculations of spatial profiles of transport parameters along the structure and the model is an unique one as the spatial DOS distributions may be included in model calculations. For the first time, the model solved an influence of diffusion currents on *I-V* characteristics.

Plasma polymerized organosilicon films constitute a class of materials with a rich and varied scientific background. This class of materials possesses a special characteristic, which distinguishes it from other plasma polymers. It is the ability to vary and control the degree of organic/inorganic character (that is, the carbon content) by appropriate choice of fabrication variables. This allows one to control many physico-chemical properties over wide ranges resulting in an extraordinary potential for useful applications, which are now only beginning to be tapped.

Plasma surface modification is an effective technique to influence physical and chemical properties of interphases in fiber reinforced polymer composites. The tensile strength of single fibers is

sensitive to both the plasma treatment and plasma polymerization. The plasma treatment changes surface morphology of fibers increasing the roughness of surfaces and thus increasing the surface area, which may result in an improving of the adhesion between reinforcing fibers and matrices. Strong adhesion is promoted by increasing the surface energy of fibers, as a result of plasma modification, decreasing its contact angle so that the wettability of fibers with the polymer matrix is improved. The chemical composition of the fiber surfaces can be changed by the plasma technology as well. The strength of composites is enhanced introducing excited and/or polar groups. An introduction of moieties available for a specific composite system is favorable to form strong chemical bonds between the fiber and the matrix. An improvement of the bonding often results in an increase in the shear strength at the expense of the impact strength.

The aim is to produce a composite with the optimal strength and toughness with respect to industrial application of the material. This may be achieved forming a controlled interphase for a specific composite system (fiber-matrix). Therefore, the surface treatment in itself is an insufficient technique, and only a coating technique capable prepare defined interlayers with a high accuracy has a chance. The interphase should be a multilayer with a strong bonding to the fiber and matrix, wherein the chemical, physical, and mechanical properties vary continuously into properties of the bulk matrix. Properties of the interphase at outer interfaces may be conformable, in chemical and physical sense, to those of the bulk fiber and bulk matrix. The bulk interphase may be a flexible material able to absorb energy and eliminate stress concentration. We believe the plasma surface modification is the true technique for attempts with controlled interphases, although we are still at the beginning.

References

1.   Hippler R., Pfau S., Schmidt M., and Schoenbach K.H. Low Temeperature Plasma Physics. Berlin: Wiley-VCH 2001.
2.   Hoffman D.M, Singh B., Thomas J.H. Handbook of Vacuum Science and Technology. London: Academic Press, 1997.
3.   Chen I. and Jansen F. *J. Non-Cryst. Solids* **59-60** (1983) 695.
4.   Chittick, R. C., Alexander, J. H., and Sterling, H. F. *J. Electrochem*. Soc. **116** (1969) 77.
5.   Spear, W.E. and LeComber, P. G. *Solid State Commun.* **17** (1975) 1193.
6.   Schröder, B. *Materials Science and Engineering* **A139** (1991) 319.
7.   Cech, V. *J. Appl. Phys.* **88** (2000) 5374.
8.   Rose, A. *Phys. Rev.* **97** (1955) 1538.
9.   Lampert, M.A. *Phys. Rev.* **103** (1956) 1648.
10. Lampert, M.A. and Mark, P. Current Injection in Solids. Academic Press, New York 1970.
11. Pfister, J.C. *Phys. Status Solidi* **A24** (1974) K15.
12. Manfredotti, C., De Blasi, C., Galassini, S., Micocci, G., Ruggiero L., and Tepore, A. *Phys. Status Solidi* **A36** (1976) 569.
13. Stöckmann, F. *Phys. Status Solidi* **A64** (1981) 475.
14. Weisfield, R.L. *J. Appl. Phys.* **54** (1983) 6401.
15. Nešpùrek, S. and Sworakowski, J. *Phys. Status Solidi* **A41** (1977) 619.
16. Nešpùrek, S. and Sworakowski, J. *Phys. Status Solidi* **A49** (1978) K149.
17. Nešpùrek, S. and Sworakowski, J. *J. Appl. Phys.* **51** (1980) 2098.
18. Böer, W. den *J. Phys., Paris* **42**, C4 (1981) 451.
19. Ralston, A. A First Course in Numerical Analysis. McGraw-Hill Book Company, NewYork 1965.
20. „ech, V., Schauer, F., and Stuchlík, J., *J. Non-Cryst. Solids* **227-230** (1998) 185.
21. „ech, V., and Stuchlík, J., *Phys. Status Solidi* **A187** (2001) 487.
22. Solomon, I. *J. Non-Cryst. Solids* **190** (1995) 107.
23. Yasuda H. Plasma Polymerization, Orlando, Academic Press, 1985.
24. Inagaki N., Plasma Surface Modification and Plasma Polymerization, Lancaster, Technomic Publ., 1996.
25. Biederman H. and Osada Y., *Plasma Polymerization Processes*, New York, Elsevier, 1992.
26. Wrobel, A. M. and Wertheimer, M. R., In Plasma Deposition, Treatment, and Etching of Polymers (Ed. R.D. Agostino), New York, Academic Press, 1990, pp. 163-268.
27. Segui, Y., @Plasma deposition from organosilicon monomers@, *Proc. NATO ASI Plasma Processing of Polymers* (Eds. R.D. Agostino, P. Favia, and F. Fracassi), Acquafredda di Maratea, Kluwer Academic Publ., 1997, pp. 305-319.
28. Cech, V., Horvath, P., Jancar, J., Schauer, F., and Nespurek, S., *Macromolecular Symposia*, **148** (1999) 321-332.
29. Gengenbach, T. R. and Griesser, H. J., *J. Polym. Sci., Part A: Polym. Chem.* **36** (1998) 985.
30. Nagai, H., Nakata, Y., Suzuki, M., and Okutani, T., *J. Mater. Sci.* **33** (1998) 1897.
31. Suzuki, M., Nakata, Y., Nagai, H., Goto, K., Nishimura, O., and Okutani, T., *Mater. Sci. Eng.*, **A246** (1998) 36.
32. Mackie, N. M., Castner, D. G., and Fisher, E. R, *Langmuir* **14** (1998) 1227.
33. Cech,V., Horvath,P., Trchova,M., Zemek, J., and Matejkova,J., *Journal of Applied Polymer Science* **82** (2001) 2106.
34. Assink, R. A., Hays, A. K., Bild, R. W., and Hawkins, B. L., *J. Vac. Sci. Techol. A*, **3**, (1985) 2629.

35. Klaptchenko, V. I. , unp V. Cech ublished results.
36. Balkova, R., Prikryl, R., Cech, V., and O. Salyk, Proc. 15th Int. Symposium on Plasma Chemistry, July 9-13, 2001, Orleans, France, Vol. 5, pp.1747.
37. Wu Souheng, Polymer Interface and Adhesion, Marcel Dekker, New York 1982.
38. Kloubek, J., *Advances in Colloid and Interface Sci*. **38** (1192) 99.
39. Cech, V., Proc. FRC 2000, September 13-15, 2000, Newcastle, UK, pp.246.
40. Sharpe, L. H.@Interfaces, interphases and adhesion: a perspective@, *Proc. NATO ASI The Interfacial Interactions in Polymeric Composites* (Ed. G. Akovali), Antalya/Kemer, Kluwer Academic Publ., 1993, pp. 1-20.
41. Kim, J-K., and Mai, Y-W., Engineered Interfaces in Fiber Reinforced Composites, Amsterdam, Elsevier, 1998.
42. Kim, J-K., and Mai, Y-W.,@Interfaces in composites@, *Structure and Properties of Fiber Composites* (Ed. T.W. Chou), Series Vol.13, VCH Publishers, 1993, pp. 239-289.
43. Li, R., Ye, L., and Mai, Y-W., *Composites* **28A** (1997) 73.
44. Hull D. and Clyne, T.W., An Introduction to Composite Materials, Cambridge, Cambridge University Press, 1996.
45. Bettge D.J. and Hinrichsen, G., *Compos. Sci. Technol*., **44** (1992) 185.
46. Weisweiler, W., Proc. NATO ASI *The Interfacial Interactions in Polymeric Composites* (Ed. Akovali, G.), Antalya/Kemer, Kluwer Academic Publ., 1993, pp. 269.
47. Jang, J. and Kim, H., *Polym. Compos*. **18** (1997) 125.
48. Kim, J.K. and Mai,Y.W., *Compos. Sci. Technol*. **41** (1991) 333.
49. Broutman, L.J. and Agarwal, B.D., *Eng. Sci* **14** (1974) 581.
50. Hancox, N.L. and Wells,H., *Fiber. Sci. Technol*. **10** (1977) 9.
51. Labronici, M. and Ishida, H., *Comp. Interfaces* **2** (1994) 199.
52. Bader MG., The composite market. In: Comprehensive Composite Materials (Kelly A., Zweben C., editors). Amsterdam: Elsevier, 2000, Volume 6.
53. Dwight DW. Glass fiber reinforcements. In: Comprehensive Composite Materials (Kelly A., Zweben C., editors.). Amsterdam: Elsevier, 2000, Volume 1.
54. Nishioka GM, *J Non-Cryst Solids* **120** (1990)102.
55. Wang W, Dibenedetto AT. *J Adhesion* **68** (1998) 183.
56. Plueddemann, EP. Silane Coupling Agents. New York: Plenum Press, 1991.
57. Thomason J. L., *Composites* **26** (1995) 487.
58. Cech, V., *Composites Part A* (2001) (submitted).
59. Sheu, G.S. and Shyu, S.S., *J. Adhesion Sci. Technol*. **9** (1994) 1027
60. Lee, S.-G., Kang, T.-J., and Yoon, T.-H., *J. Adhesion Sci. Technol*. **12** (1998) 731.

Anotace

Hydrogenovaný amorfní křemík (a-Si:H) je tenkovrstvý polovodičový materiál s vynikajícími vlastnostmi. Může být vyroben velice snadno a s nízkými náklady přípravou z plynné fáze v plazmatu. Vysoce kvalitní materiál lze snadno a efektivně dotovat během výroby a snadno lze vytvářet také slitiny, což předurčuje tento materiál pro široké pole aplikací. Autor ve svých pracích vyvinul nástroje (metody a techniky) pro úspěšné vyhodnocení hustoty lokalizovaných elektronických stavů v materiálu, nejdůležitějšího materiálového parametru pro a-Si:H, z ustálených a relaxačních proudů omezených prostorovým nábojem. Autorem navržený model struktury n^+-i-n^+ založený na numerických simulacích umožňuje výpočet průběhu transportních parametrů podél struktury a navíc jeho jedinečnost spočívá v možnosti volby prostorového rozložení hustoty stavů ve struktuře. Tento model jako první úspěšně řeší otázku vlivu difúzních proudů na průběh volt-ampérových charakteristik použité struktury.

Organokřemičité tenké vrstvy připravené polymerací v plazmatu zahrnují skupinu materiálů s velice bohatým a rozmanitým technologickým potenciálem přípravy materiálu. Tato skupina materiálů má zvláštní rys, který ji odlišuje od ostatních plazmových polymerů. Touto zvláštností je možnost měnit a řídit poměr mezi organickým a anorganickým charakterem materiálu (daného obsahem uhlíku) vhodnou volbou výrobních parametrů. To umožňuje řídit mnohé fyzikálně-chemické vlastnosti materiálu v poměrně širokých mezích, což zase nabízí širokou škálu možných aplikací, které začínají být teprve nyní využívány.

Plazmová polymerace je efektivní technologií pro povrchové úpravy vláken vyztužujících polymerní matrice. Tato technologie umožňuje ovlivňovat fyzikální a chemické vlastnosti kompozitní mezifáze. Pevnost vláken v tahu je citlivá jak na plazmové povrchové úpravy, tak na plazmovou polymeraci. Plazmové povrchové úpravy mění povrchovou morfologii vláken, zvyšují drsnost povrchu a tím také kontaktní plochu vláken, což může vést ke zlepšení adheze mezi vyztužujícími vlákny a matricí. Silná adheze je podpořena zvýšením povrchové energie vláken, jako důsledek plazmové úpravy, kdy klesá kontaktní úhel tak, že smáčivost vláken polymerní matricí je zvýšena. Rovněž chemické složení vláken na povrchu je možné měnit plazmovou úpravou. Pevnost kompozitního materiálu je zvýšena vytvořením excitovaných a polárních skupin na povrchu vláken. Nicméně, zvýšení adheze často vede ke zvýšení smykové pevnosti mezifáze a také pevnosti kompozitního materiálu, ale na úkor jeho houževnatosti.

Cílem je připravit kompozit s optimální pevností a houževnatostí vzhledem k průmyslovému použití tohoto materiálu. Toho lze dosáhnout vytvořením řízené mezifáze pro specifický kompozitní systém (vlákno-matrice). Tedy, plazmová povrchová úprava jako taková není schopna tyto požadavky zajistit, ale tyto nároky může splnit plazmová polymerace, pokud bude schopna připravit mezivrstvu o požadovaných vlastnostech s dostatečnou přesností. Kompozitní mezifáze by měla být multivrstva dobře provázaná jak s vláknem, tak i matricí, jejíž fyzikální a chemické vlastnosti se spojitě mění mezi vláknem a matricí. Mezivrstva by měla být tvořena dostatečně pružným materiálem, který je schopen absorbovat energii a snížit napětí na rozhraních. Věříme, že plazmová polymerace je vhodnou technologií pro účely pokusů o řízenou mezifázi, ačkoliv jsme teprve na začátku tohoto procesu.